

# Antibunching of microwave-frequency photons observed in correlation measurements using linear detectors

D. Bozyigit<sup>1</sup>, C. Lang<sup>1</sup>, L. Steffen<sup>1</sup>, J. M. Fink<sup>1</sup>, C. Eichler<sup>1</sup>, M. Baur<sup>1</sup>, R. Bianchetti<sup>1</sup>, P. J. Leek<sup>1</sup>, S. Filipp<sup>1</sup>, M. P. da Silva<sup>2</sup>, A. Blais<sup>2</sup> and A. Wallraff<sup>1\*</sup>

**At optical frequencies the radiation produced by a source, such as a laser, a black body or a single-photon emitter, is frequently characterized by analysing the temporal correlations of emitted photons using single-photon counters. At microwave frequencies, however, there are no efficient single-photon counters yet. Instead, well-developed linear amplifiers allow for efficient measurement of the amplitude of an electromagnetic field. Here, we demonstrate first- and second-order correlation function measurements of a pulsed microwave-frequency single-photon source integrated on the same chip with a 50/50 beam splitter followed by linear amplifiers and quadrature amplitude detectors. We clearly observe single-photon coherence in first-order and photon antibunching in second-order correlation function measurements of the propagating fields.**

In quantum optics<sup>1</sup>, the single-photon detector is a versatile tool to explore the properties of radiation emitted from a variety of classical and quantum sources. At optical frequencies these detectors easily produce a ‘click’ when a single photon impinges on them. Recording the statistics of such events, one is able to measure not only the average number of emitted photons  $n = \langle a^\dagger a \rangle$  but also higher-order statistical correlations between the emitted photons. Here,  $a^\dagger$  and  $a$  are the creation and annihilation operators of the radiation detected in a given mode. At lower frequencies, such as in the microwave-frequency domain, however, no efficient single-photon detectors exist yet, as photons at these frequencies carry an energy that is orders of magnitude less than at optical frequencies. Instead, at microwave frequencies, linear amplifiers followed by an instrument recording a voltage, such as an oscilloscope, are commonly used to detect small-amplitude electromagnetic fields. Such amplifiers have several orders of magnitude gain but necessarily add noise to the signal<sup>2</sup>. Nevertheless, valuable information about the properties of quantum radiation sources in this frequency range can be acquired. With sufficient averaging, electric-field amplitudes that are proportional to the sum and difference of the field operators  $a$  and  $a^\dagger$  can be detected in this way, even at the single-photon level<sup>3</sup>. We demonstrate here that by recording the full time series of the detected signal—instead of its time average—and using efficient digital signal processing, we can extract characteristic correlation functions of radiation generated by microwave-frequency emitters such as a single-photon source.

For our experiments we have integrated a microwave-frequency single-photon source, similar to the one presented in ref. 3, with an on-chip 50/50 beam splitter<sup>4–6</sup> in a single superconducting electronic circuit (see Fig. 1a). We coherently and controllably couple a single qubit to an asymmetric high-quality resonator to emit an individual photon on demand into a single output mode  $c$  (see Fig. 1). At the same time, this mode is one of the two input modes of a microwave-frequency beam splitter

with the other mode  $d$  prepared approximately in the vacuum state using an attenuator thermalized at 20 mK. The microwave beam splitter creates two equal-amplitude output modes  $e$  and  $f$  and obeys the usual quantum optics input–output relations<sup>1,5,7</sup>. The superconducting transmon qubit<sup>8</sup> used in this experiment is characterized by its maximum Josephson energy  $E_{J,\max} \approx 20.7$  GHz, its charging energy  $E_C \approx 440$  MHz and its energy relaxation and dephasing times in excess of a few hundred nanoseconds. The transition frequency of the qubit is flux tunable using both a quasi-static magnetic field generated with a miniature coil and an on-chip transmission line to generate nanosecond-timescale flux pulses. By integrating our qubit into a superconducting coplanar transmission line resonator of frequency  $\nu_r \approx 6.763$  GHz and quality factor  $Q \approx 1,690$ , we couple it strongly to a single mode  $a$  of the radiation field stored in the resonator. This approach is known as circuit quantum electrodynamics<sup>9</sup> and allows one to study in exquisite detail the interaction of quantum two-level systems with quantized radiation fields.

In this system we have implemented a single-photon source using the following scheme. Applying a phase-controlled truncated Gaussian microwave pulse of variable amplitude  $A_r$  and total duration  $t_r = 12$  ns to the qubit biased at a transition frequency of  $\nu_q = 8.052$  GHz, we prepare an arbitrary superposition state  $|\psi_q\rangle = \alpha|g\rangle + \beta|e\rangle$  between the qubit ground  $|g\rangle$  and excited state  $|e\rangle$ . The superposition is characterized by the two complex probability amplitudes  $\alpha = \cos(\theta_r/2)$  and  $\beta = \sin(\theta_r/2)e^{i\phi}$  that are parameterized by the polar (Rabi) angle  $\theta_r \propto A_r$  and the phase angle  $\phi$ . We characterize the qubit state using a pulsed dispersive measurement of the resonator transmission<sup>10</sup> and clearly observe Rabi oscillations in the qubit population  $P_e$  versus the amplitude  $A_r$  (not shown). After the qubit state preparation, we apply a current pulse of controlled amplitude and duration to the flux bias line to tune the qubit transition frequency into resonance with the resonator frequency  $\nu_r$ . We time-resolve the resonant

<sup>1</sup>Department of Physics, ETH Zürich, CH-8093, Zürich, Switzerland, <sup>2</sup>Département de Physique, Université de Sherbrooke, Sherbrooke, Québec, J1K 2R1, Canada. \*e-mail: andreas.wallraff@phys.ethz.ch.

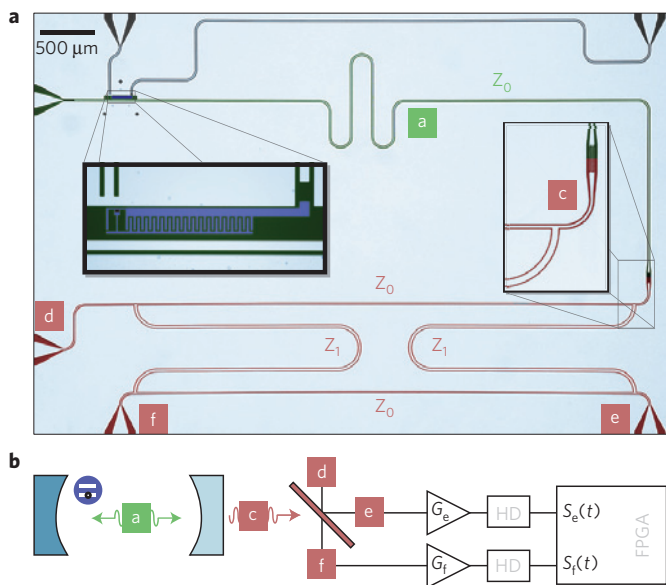


**Figure 1 | Sample and schematic of the experimental set-up.**

**a**, Superconducting coplanar waveguide resonator (green) realizing resonant mode a interacting with integrated transmon qubit (left inset) that can be biased with large-bandwidth flux and charge gate lines (top inputs). Output mode c is coupled into the beam splitter (red) with mode d in the vacuum state and output modes e and f. Four  $\lambda/4$  sections of waveguide with impedances  $Z_0 = 50 \Omega$  and  $Z_1 = 50/\sqrt{2} \Omega$  realize the beam splitter. **b**, Schematic of resonator with two-level system generating a photon in mode a, emitting it into mode c onto a beam splitter with modes d, e and f. Linear amplifiers with gain  $G_{e,f}$  are coupled to both beam-splitter outputs amplifying the radiation in modes e and f. Heterodyne detectors (HD) extract both quadratures of the output fields and feed results to FPGA-based digital correlation electronics.

vacuum Rabi oscillations of the coupled system at a frequency of  $2g/(2\pi) = 146 \text{ MHz}$  by dispersively measuring the qubit state after it has been tuned back to the frequency  $\nu_q$  strongly detuned from the resonator. Adjusting the qubit–resonator interaction time  $t_{vr} = \pi/(2g) = 3.4 \text{ ns}$  to half a vacuum Rabi period, we coherently map the qubit state  $|\psi_q\rangle$  to an equivalent superposition state  $|\psi_c\rangle = \alpha|0\rangle + \beta|1\rangle$  of the  $|0\rangle$  and  $|1\rangle$  photon Fock states stored in the resonator mode a. Similar techniques have been used to prepare and measure a wide range of intracavity photon superposition states in recent experiments both with superconducting circuits<sup>11</sup> and with Rydberg atoms<sup>12</sup>.

In a next step, we characterize zero- and one-photon superposition states by measuring the quadrature amplitudes of the microwave fields emitted from the cavity into the output mode c. For this purpose we have realized a set-up in which we independently and simultaneously detect the field of both output modes of the beam splitter e and f (see Fig. 1b). Our measurement scheme comprises two independent detection chains similar to the one discussed in ref. 5. Each chain consists of a cold amplifier with gain  $G_{e,f} \approx 39 \text{ dB}$  and noise temperature  $T_{N(e,f)} \approx 3.0 \text{ K}$  followed by a two-stage heterodyne detector in which the signal is down-converted from the resonator frequency to 25 MHz in an analog stage and to d.c. in a digital homodyne stage. In this way, we extract the complex envelope<sup>13</sup>  $S_{e,f}(t)$  of the amplified electric field  $E_{e,f}^{(+)}$  described by

$$E_{e,f}^{(+)}(t) + N_{e,f}(t) = S_{e,f}(t)e^{-2\pi i\nu_r t}$$

where the real and imaginary parts of  $S_{e,f}(t)$  are the two field quadrature amplitudes in the frame rotating at the resonator

frequency and  $N_{e,f}(t)$  includes the vacuum noise and the noise added by the amplifiers<sup>14</sup>.

As a first example, we present a measurement of the time dependence of the quadrature amplitudes of the electric field in one output mode (e) of the beam splitter. Ensemble averaging over  $10^7$  realizations gives us access to the expectation value of the annihilation operator of the cavity field  $\langle S_e(t) \rangle \propto \langle a(t) \rangle$  (ref. 14). Similar measurements carried out directly at the output of the cavity without a beam splitter were presented in ref. 3, where the cavity photon was created by Purcell-limited spontaneous emission. Figure 2a shows the real part of  $\langle S_e(t) \rangle$  versus time  $t$  after the preparation of the photon superposition state  $|\psi_c\rangle$  characterized by the qubit Rabi angle  $\theta_r$  used for its preparation. We find excellent agreement with the expected average field quadrature amplitude  $\langle a \rangle \propto \sin(\theta_r)/2$  (Fig. 2c). In particular, we observe the largest signals for the superposition states  $|\psi_c^+\rangle = (|0\rangle + |1\rangle)/\sqrt{2}$  and  $|\psi_c^-\rangle = (|0\rangle - |1\rangle)/\sqrt{2}$  prepared with  $\theta_r = \pi/2$  and  $3\pi/2$ , respectively. As expected from the uncertainty principle, the Fock states  $|0\rangle$  and  $|1\rangle$  prepared with  $\theta_r = 0$  and  $\pi$ , respectively, do not show any quadrature amplitude signals (Fig. 2a) because the phase of these number states is completely uncertain. For all of the above measurements, the overall global phase of the signals is adjusted such that the imaginary part of  $S_e(t)$  is equal to zero, which therefore is not shown. We also note that the amplifier noise averages to zero in the quadrature amplitude measurement.

Moreover, the time dependence of all measurement traces is well understood, see for example the state  $|\psi_c^+\rangle$  in Fig. 2b. A model accounting for an exponential decay with time constant  $2T_\kappa = Q/\pi\nu_r = 80 \text{ ns}$  and the limited detection bandwidth of 15 MHz explains the temporal shape of the data accurately (red line). Note that the rise time is not limited by the state-preparation time  $t_{vr} = 3.4 \text{ ns}$  but by the detection bandwidth.

In our measurement scheme, we simultaneously record the time-dependent quadrature amplitudes  $S_{e,f}(t)$  detected at both output ports of the beam splitter continuously for each single photon generated. Using input–output theory<sup>15</sup>, one can show that the full information about the intracavity mode a is contained in the moments and cross-correlations of  $S_{e,f}(t)$  (ref. 14). Conventionally, the statistical moments of this kind of heterodyne quadrature data are associated with the statistical moments of antinormally ordered field operators<sup>1</sup>. In many cases, however, one is used to working with normally ordered expectation values such as photon number, first- and second-order correlation functions. We demonstrate that these moments can be obtained efficiently by applying the correct algebraic transformations on the full measurement record  $S_{e,f}(t)$  of the two detection channels before carrying out ensemble averaging<sup>14,16</sup>.

This technique is realized using a two-channel analog-to-digital converter with a time resolution of 10 ns. On the basis of the measurement record of each event, we can then calculate any expectation value, such as averages, products or correlations, that can be expressed in terms of the detected output signals  $S_{e,f}(t)$ . Processing these data in real time using field-programmable gate array (FPGA) electronics allows us to efficiently extract information even in the presence of substantial noise added by the amplifiers.

Taking advantage of this versatile scheme, we digitally calculate—instead of using a diode as a power meter in which the detection and the averaging is realized within the detector<sup>3</sup>—the expectation value of the instantaneous power  $\langle S_e^*(t)S_e(t) \rangle$  transmitted into one output mode (e) of the beam splitter with the cavity mode a prepared in the Fock state  $|1\rangle$  (not shown). In the direct power measurement, the detected noise power of the amplifier dominates by a factor of about 700 over the single-photon power, which is still observable using sufficient averaging. From this measured background noise we determine the

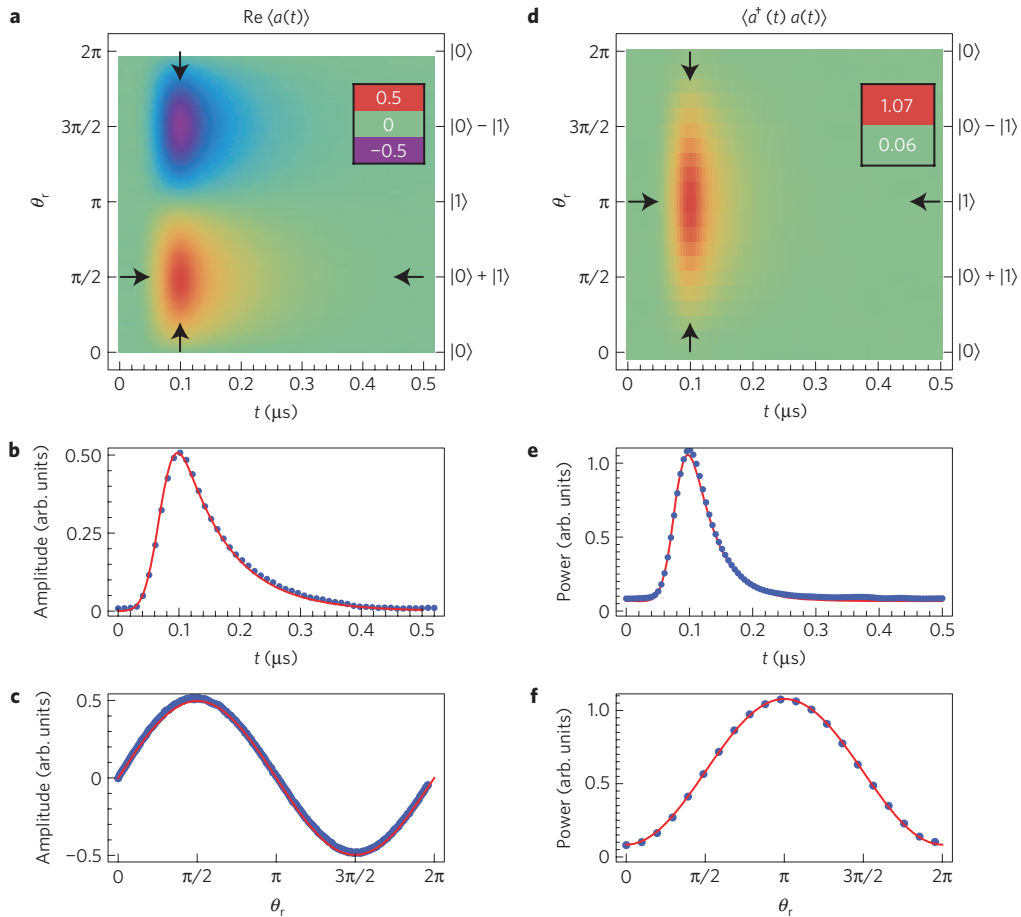


**Figure 2 | Quadrature amplitude and cross-power measurements.** **a**, Time dependence of cavity field quadrature amplitude measured at output mode *e* of the beam splitter for zero- and one-photon superposition states characterized by the Rabi angle  $\theta_r$  (left axis) or equivalently the generated state (right axis). **b**, Single quadrature trace at  $\theta_r = \pi/2$  corresponding to  $(|0\rangle + |1\rangle)/\sqrt{2}$  (horizontal arrows in **a**). **c**, Dependence of maximum quadrature amplitude on  $\theta_r$  at time  $t$  indicated by vertical arrows in **a**. **d**, Measured time dependence of cross-power between modes *e* and *f* for the same preparation as in **a**. **e**, Single power trace at  $\theta_r = \pi$  corresponding to  $|1\rangle$  (horizontal arrows in **d**). **f**, Dependence of maximum cross-power on  $\theta_r$  at time  $t$  indicated by vertical arrows in **d**. The blue dots are data, and the red lines are models explained in the text.

system noise temperature  $T_{N(\text{sys})} \approx 10.6$  K of our detection chain with respect to the output of the resonator.  $T_{N(\text{sys})}$  is substantially higher than the noise temperature of the amplifiers because of absorption in the cables and insertion loss of components in the detection chain.

Calculating the cross-power  $\langle S_e^*(t)S_f(t) \rangle$  between the two output modes of the beam splitter instead of the direct power detected in just a single mode, we can effectively reject the noise added by the amplifiers in our measurement scheme. The detected cross-power is related to the average photon number in the cavity as<sup>14</sup>

$$\langle S_e^*(t)S_f(t) \rangle \propto \langle a^\dagger(t)a(t) \rangle + P(N_{ef})$$

where  $P(N_{ef})$  is the power of correlated noise between channels *e* and *f*. In these measurements, the detected noise cross-power has a characteristic noise temperature of only 80 mK, much smaller than the characteristic noise temperature of the direct noise power of each amplifier, indicating that the two detection chains add predominantly uncorrelated noise. The residual correlations result from weak thermal radiation at the vacuum port *d* and technical origins, such as insufficient isolation of the two detection chains.

We have characterized the measured cross-power of our single-photon source for the same set of cavity superposition states as used for the quadrature amplitude measurements averaging over  $6.7 \times 10^8$  photon state preparations (Fig. 2d). We find excellent

agreement of the temporal evolution of the cavity photon number (Fig. 2e) as a function of the preparation angle of the photon state  $\langle a^\dagger a \rangle \propto \sin^2(\theta_r/2)$  (Fig. 2f). The maximum cross-power is measured for the Fock state  $|1\rangle$  ( $\theta_r = \pi$ ) and the minimum power for the  $|0\rangle$  state ( $\theta_r = 0$  or  $2\pi$ ) (Fig. 2d).

Finally, we have characterized our single-photon source using measurements of the time-dependent first-order cross-correlation

$$\Gamma^{(1)}(\tau) = \int \langle S_e^*(t)S_f(t+\tau) \rangle dt$$

of the signals  $S_e$  and  $S_f$  in the two output modes and an autocorrelation of the cross-power

$$\Gamma^{(2)}(\tau) = \int \langle S_e^*(t)S_e^*(t+\tau)S_f(t+\tau)S_f(t) \rangle dt \quad (1)$$

Here,  $\Gamma^{(1)}$  is a direct measure of the first-order correlation function  $G^{(1)}$  and  $\Gamma^{(2)}$  is a direct measure of the second-order correlation function  $G^{(2)}$  of the resonator field<sup>14</sup>.

For the measurement, we generate a train of 40 single-photon pulses each created using the procedure described above and with a pulse separation of  $t_p = 512$  ns, which is much greater than the qubit and cavity decay times. To remove the small correlated noise background, we subtract the measured correlation function  $\Gamma_{ss}^{(1)}(\tau)$  in the resonator steady state from the signal  $\Gamma^{(1)}(\tau)$  acquired when

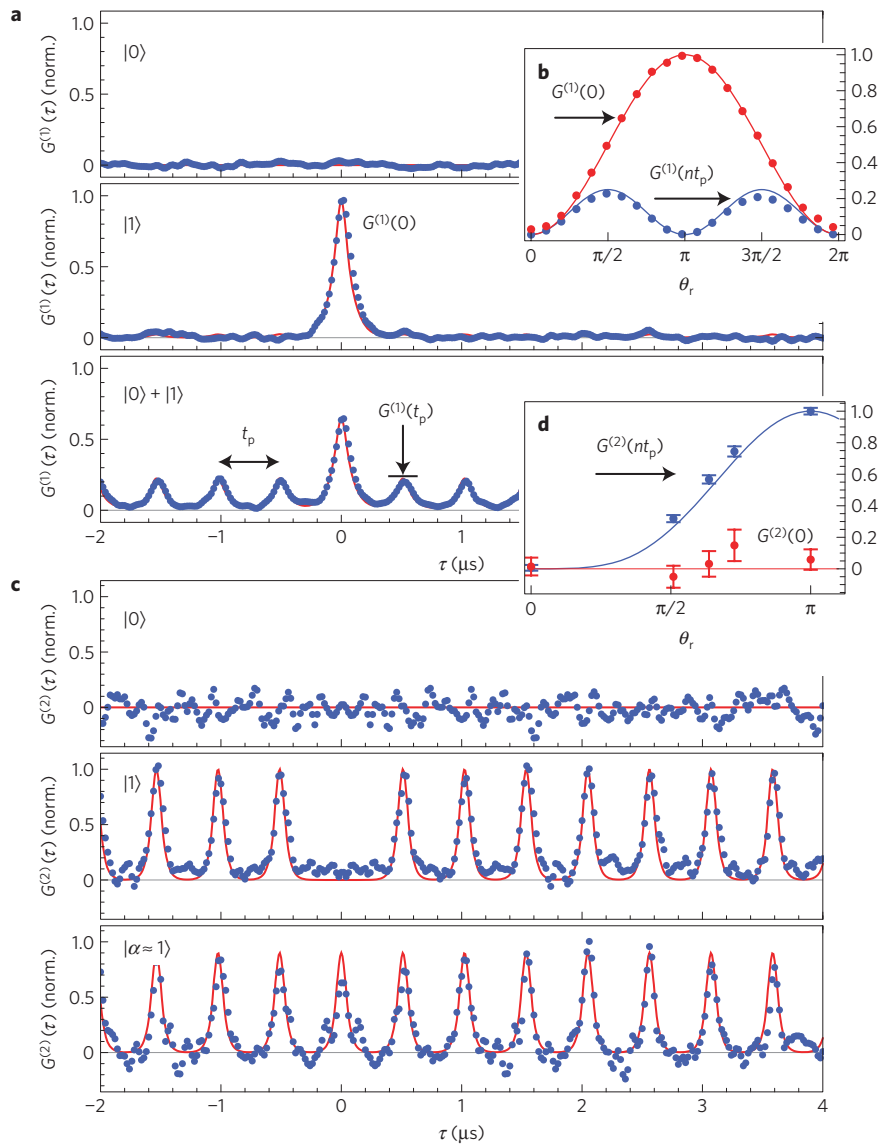


**Figure 3 | Correlation function measurements.** **a**, Time dependence of first-order correlation function  $G^{(1)}(\tau)$  of the cavity field for the indicated states. **b**,  $G^{(1)}(0)$  and  $G^{(1)}(nt_p)$  versus  $\theta_r$ . **c**, Measured second-order correlation function  $G^{(2)}(\tau)$  for the states  $|0\rangle$  (top trace),  $|1\rangle$  (middle trace) and a coherent state  $|\alpha \approx 1\rangle$  (bottom trace). Note that the noise in these measurements is symmetric around  $\tau = 0$  in accordance with the symmetry of equation (1). **d**,  $G^{(2)}(0)$  and  $G^{(2)}(nt_p)$  versus qubit preparation angle  $\theta_r$ . The blue error bars are the inferred standard deviation of the mean  $G^{(2)}(nt_p)$ . The red error bars are the estimated standard deviation of  $G^{(2)}(0)$ . In all panels the dots are data and the lines are theoretical predictions<sup>14</sup>.

carrying out the photon state preparation sequence. From the recorded quadrature amplitude data, we calculate

$$\Gamma^{(1)}(\tau) - \Gamma_{ss}^{(1)}(\tau) \propto G^{(1)}(\tau)$$

which gives us access to the first-order correlation function  $G^{(1)}(\tau) = \int \langle a^\dagger(t)a(t+\tau) \rangle dt$  of the resonator field<sup>14</sup>. To measure each trace in Fig. 3a,  $64 \times 10^6$  trains of 40 photons were prepared in a specific state and  $G^{(1)}(\tau)$  was calculated in real time using our FPGA-based electronics, corresponding to approximately 0.5 Tbyte of data that have been evaluated in about 30 min.

The  $G^{(1)}(\tau)$  data (Fig. 3a) are characterized by a set of peaks that are separated by the repetition time  $t_p$  of the single-photon source. The amplitude of  $G^{(1)}$  at  $\tau = nt_p$ , representing the correlation between a pulse  $i$  and  $i + n$ , depends in a characteristic fashion on  $\theta_r$ . For the Fock state  $|1\rangle$  (at  $\theta_r = \pi$ ), the correlation function  $G^{(1)}(0)$  is at a maximum and vanishes at  $G^{(1)}(nt_p)$  as

there is no coherence between photons emitted from the source at different times. In fact,  $G^{(1)}(0) \propto \langle a^\dagger a \rangle \propto |\beta|^2 = \sin^2(\theta_r/2)$  oscillates sinusoidally with the preparation angle, as it essentially measures the average photon number of the generated field (Fig. 3b). However, for photon superposition states, the expectation values of  $\langle a^\dagger \rangle$  and  $\langle a \rangle$  of subsequently generated photon states have non-vanishing values, as discussed before. As photons from different repetitions of the experiments are uncorrelated,  $G^{(1)}(nt_p) \propto \langle a^\dagger \rangle \langle a \rangle$  has a finite value and oscillates at half the period. Thus,  $G^{(1)}(nt_p) \propto |\alpha\beta|^2 = \sin^2(\theta_r)/4$  is maximized for the states  $|\psi_c^+\rangle$  and  $|\psi_c^-\rangle$  (Fig. 3b).

The observed features of the first-order correlation function together with the results in Fig. 2 confirm that the procedure implemented for generating single-photon pulses performs as expected. Measurements of the second-order correlation function  $G^{(2)}(\tau)$  then do provide unambiguous proof of the quantum character of the generated propagating field, independent of any prior knowledge about its source<sup>1</sup>. On the basis of the results

presented in ref. 14, we obtain the second-order correlation function  $G^{(2)}(\tau)$  by measuring

$$\Gamma^{(2)}(\tau) - \Gamma_{ss}^{(2)}(\tau) \propto G^{(2)}(\tau)$$

where  $\Gamma_{ss}^{(2)}(\tau)$  is the steady-state measurement. Measurements of  $G^{(2)}(\tau)$  averaged over  $5 \times 10^9$  to  $9 \times 10^9$  trains of 40 photon state preparations are shown in the three panels of Fig. 3c. For the vacuum state  $|0\rangle$ , we find  $G^{(2)}(\tau) = 0$  everywhere, as expected. For the Fock state  $|1\rangle$ , we observe a characteristic set of peaks in  $G^{(2)}(\tau)$  spaced by the repetition time  $t_p$  of the source with a strongly suppressed peak  $G^{(2)}(\tau = 0) \approx 0.1 \ll 1$  at zero delay time. This measurement clearly demonstrates antibunching of the radiation emitted by our single-photon source as  $G^{(2)}(0) \ll G^{(2)}(nt_p)$ . At the same time these measurements demonstrate that the non-classical properties of the radiation are fully retained in the detection process in the form of statistical correlations between the single-shot quadrature amplitudes detected behind the beam splitter.

To further compare our results with the theoretical predictions, we have carried out the same  $G^{(2)}(\tau)$  measurement for three additional photon superposition states as parameterized by the Rabi angle  $\theta_r$ . Here we note that  $G^{(2)}(\tau)$  is normalized such that the average peak height for the prepared state  $|1\rangle$  is equal to unity. For all prepared states, we observe the expected scaling of  $G^{(2)}(nt_p) \propto \sin^4(\theta_r/2)$  and  $G^{(2)}(0) \approx 0$  (see Fig. 3d), confirming the measurement of antibunching.

Finally, we have applied short coherent pulses at  $\nu_r$  to the resonator input to realize a coherent source with approximately the same average intensity as the single-photon source. In a measurement of  $G^{(2)}(\tau)$ , we find the expected periodic pattern with a peak of amplitude  $\approx 0.9$  present also at  $\tau = 0$  (Fig. 3c bottom trace), which is in stark contrast to the  $|1\rangle$  state.

In quantum optics at optical frequencies, second-order correlation function measurements using single-photon detectors have a long history and are very important for characterizing many sources of light, including single-photon emitters based on atoms<sup>17</sup>, atoms in cavities<sup>18</sup>, ions<sup>19</sup>, molecules<sup>20</sup>, quantum dots<sup>21</sup> and nitrogen-vacancy centres<sup>22</sup>, to name just a few. Our experiments clearly demonstrate that correlation function measurements based on quadrature amplitude detection are a powerful tool to characterize quantum properties of propagating microwave-frequency radiation fields. Even in the presence of noise added by the amplifier, two-channel detection and efficient data processing techniques allow for the measurements of higher statistical moments of the fields. When better, possibly quantum-limited, amplifiers<sup>23</sup> become available the demonstrated techniques may help to facilitate the full tomography of propagating radiation fields. Furthermore, the flexibility of circuit design and the high level of control achievable in circuit quantum electrodynamics will enable future experiments with propagating quantum microwave fields for basic research and applications taking advantage of correlation function measurements and making use of integrated linear optics elements such as beam splitters or interferometers.

Received 9 June 2010; accepted 11 October 2010; published online 5 December 2010

## References

1. Walls, D. & Milburn, G. *Quantum Optics* (Springer, 1994).
2. Caves, C. M. Quantum limits on noise in linear amplifiers. *Phys. Rev. D* **26**, 1817–1839 (1982).

3. Houck, A. *et al.* Generating single microwave photons in a circuit. *Nature* **449**, 328–331 (2007).
4. Pozar, D. M. *Microwave Engineering* (Addison-Wesley, 1993).
5. Gabelli, J. *et al.* Hanbury Brown–Twiss correlations to probe the population statistics of GHz photons emitted by conductors. *Phys. Rev. Lett.* **93**, 056801 (2004).
6. Mariantoni, M. *et al.* Planck spectroscopy and quantum noise of microwave beam splitters. *Phys. Rev. Lett.* **105**, 133601 (2010).
7. Menzel, E. P. *et al.* Dual-path state reconstruction scheme for propagating quantum microwaves and detector noise tomography. *Phys. Rev. Lett.* **105**, 100401 (2010).
8. Koch, J. *et al.* Charge-insensitive qubit design derived from the Cooper pair box. *Phys. Rev. A* **76**, 042319 (2007).
9. Wallraff, A. *et al.* Strong coupling of a single photon to a superconducting qubit using circuit quantum electrodynamics. *Nature* **431**, 162–167 (2004).
10. Bianchetti, R. *et al.* Dynamics of dispersive single-qubit readout in circuit quantum electrodynamics. *Phys. Rev. A* **80**, 043840 (2009).
11. Hofheinz, M. *et al.* Synthesizing arbitrary quantum states in a superconducting resonator. *Nature* **459**, 546–549 (2009).
12. Deleglise, S. *et al.* Reconstruction of non-classical cavity field states with snapshots of their decoherence. *Nature* **455**, 510–514 (2008).
13. Mandel, L. & Wolf, E. *Optical Coherence and Quantum Optics* (Cambridge Univ. Press, 1995).
14. da Silva, M. P., Bozyigit, D., Wallraff, A. & Blais, A. Schemes for the observation of photon correlation functions in circuit QED with linear detectors. *Phys. Rev. A* **82**, 043804 (2010).
15. Gardiner, C. W. & Collett, M. J. Input and output in damped quantum systems: Quantum stochastic differential equations and the master equation. *Phys. Rev. A* **31**, 3761–3774 (1985).
16. Grosse, N. B., Symul, T., Stobinska, M., Ralph, T. C. & Lam, P. K. Measuring photon antibunching from continuous variable sideband squeezing. *Phys. Rev. Lett.* **98**, 153603 (2007).
17. Kimble, H. J., Dagenais, M. & Mandel, L. Photon antibunching in resonance fluorescence. *Phys. Rev. Lett.* **39**, 691–695 (1977).
18. Kuhn, A., Hennrich, M. & Rempe, G. Deterministic single-photon source for distributed quantum networking. *Phys. Rev. Lett.* **89**, 067901 (2002).
19. Diedrich, F. & Walther, H. Nonclassical radiation of a single stored ion. *Phys. Rev. Lett.* **58**, 203–206 (1987).
20. Basché, T., Moerner, W. E., Orrit, M. & Talon, H. Photon antibunching in the fluorescence of a single dye molecule trapped in a solid. *Phys. Rev. Lett.* **69**, 1516–1519 (1992).
21. Michler, P. *et al.* A quantum dot single-photon turnstile device. *Science* **290**, 2282–2285 (2000).
22. Kurtsiefer, C., Mayer, S., Zarda, P. & Weinfurter, H. Stable solid-state source of single photons. *Phys. Rev. Lett.* **85**, 290–293 (2000).
23. Castellanos-Beltran, M. A., Irwin, K. D., Hilton, G. C., Vale, L. R. & Lehnert, K. W. Amplification and squeezing of quantum noise with a tunable Josephson metamaterial. *Nature Phys.* **4**, 929–931 (2008).

## Acknowledgements

We thank T. Frey and G. Littich for their contributions at the early stages of the project. We also thank C. M. Caves, D. Esteve and especially K. W. Lehnert for very fruitful discussions and J. Blatter for comments on the manuscript. This work was supported by the European Research Council (ERC) through a Starting Grant and by ETHZ. M.P.d.S. was supported by a NSERC postdoctoral fellowship. A.B. was supported by NSERC, CIFAR and the Alfred P. Sloan Foundation.

## Author contributions

D.B., C.L. and L.S. carried out the experiments. D.B. and C.L. analysed the data and developed hardware data processing. J.M.F. and L.S. designed and fabricated the sample. Experiments were carried out at ETH Zurich; all authors in Zurich contributed to setting up and maintaining the cryogenic set-up, and developing measurement software. M.P.d.S. and A.B. contributed to the theoretical interpretation. A.W. and D.B. wrote the manuscript. All authors commented on the manuscript. A.W. supervised the project.

## Additional information

The authors declare no competing financial interests. Reprints and permissions information is available online at <http://npg.nature.com/reprintsandpermissions>. Correspondence and requests for materials should be addressed to A.W.